NASA TECHNICAL MEMORANDUM

NASA TM X-62,414

VELOCITY AND ROLLING-MOMENT MEASUREMENTS IN THE WAKE OF A SWEPT-WING MODEL IN THE 40- BY 80-FOOT WIND TUNNEL

Vernon J. Rossow and Victor R. Corsiglia
Ames Research Center
Moffett Field, California 94035

Richard G. Schwind
Nielsen Engineering & Research, Inc.
Mountain View, California 94043

Juanita K. D. Frick and Opal J. Lemmer
U.S. Army Air Mobility R&D Laboratory
Moffett Field, California 94035

April 1975

1. Report No. TM X-62,414	2. Government Accession No.	3. Recipient's Catalog No.
4. Title and Subtitle VELOCITY AND ROLLING-MOMENT MEASUREMENTS IN THE WAKE OF A SWEPT-WING MODEL IN THE 40- BY 80-FOOT WIND TUNNEL		5. Report Date
		6. Performing Organization Code A-5918
7. Author(s) Vernon J. Rossow, Victor R. Corsiglia, Richard G. Schwind, Juanita K. D. Frick, and Opal J. Lemmer		8. Performing Organization Report No.
		10. Work Unit No. 505-06-22
9. Performing Organization Name and Address Ames Research Center, NASA, Moffett Field, Calif. 94035; Nielsen Engineering & Research, Inc., Mt. View, Calif. 94043; U. S. Army Air Mobility R&D Laboratory, Moffett Field, Calif. 94035		11. Contract or Grant No.
		13. Type of Report and Period Covered Technical Memorandum
12. Sponsoring Agency Name and Address National Aeronautics and Space Administration Washington, D. C. 20546		14. Sponsoring Agency Code

15. Supplementary Notes

16. Abstract

Measurements were made in the wake of a swept-wing model to study the structure of lift-generated vortex wakes shed by conventional span loadings and by several span loadings designed to reduce wake velocities. Variations in the span loading on the swept-wing generator were obtained by deflecting seven flap segments on each side by amounts determined by vortex-lattice theory to approximate the desired span loadings. The resulting wakes were probed with a three-component, hot-wire probe to measure velocity, and with a wing to measure the rolling moment that would be induced on a following aircraft. The experimental techniques are described herein, and the measured velocity and rolling moments are presented, along with some comparisons with the applicable theories.

17. Key Words (Suggested by Author(s)) Aeronautics Aerodynamics Fluid Mechanics & Heat Transfer	18. Distribution Statement Unclassified — Unlimited STAR Categories 01, 02, 34

19. Security Classif. (of this report) Unclassified	20. Security Classif. (of this page) Unclassified	21. No. of Pages 36	22. Price* $3.75

NOMENCLATURE

$\mathcal{R}$	aspect ratio, b^2/S
b	span of wing
c	wing chord
$\bar{c}$	mean wing chord, S/b
C_l	rolling-moment coefficient, torque/$(\frac{1}{2} \rho U_\infty^2 Sb)$
C_ℓ	local lift coefficient
C_L	lift-coefficient, lift/$(\frac{1}{2} \rho U_\infty^2 Sb)$
C_{L_α}	lift-curve slope
P	semi-perimeter/span
q	dynamic pressure, $\frac{1}{2} \rho U_\infty^2$
r	radius
R	radius of rotor arm
S	wing area or distance along arc of rotor
t	time
u,v,w	velocity components in x,y,z directions, respectively
x,y,z	coordinate axes; x is streamwise and z is vertical
U_∞	free-stream velocity (alined with x axis)
α	angle of attack
θ	circumferential direction
Γ	circulation
ρ	air density

Subscripts

f	following model that encounters wake
g	model that generates wake

r	radial direction
v	vortex
w	wing
∞	free stream
$\mathcal{C}_L$	centerline
θ	circumferential direction

VELOCITY AND ROLLING-MOMENT MEASUREMENTS IN THE WAKE OF A

SWEPT-WING MODEL IN THE 40- BY 80-FOOT WIND TUNNEL

Vernon J. Rossow,* Victor R. Corsiglia,* Richard G. Schwind,**

Juanita K. D. Frick,*** and Opal J. Lemmer***

SUMMARY

Measurements were made in the wake of a swept-wing model to study the structure of lift-generated vortex wakes shed by conventional span loadings and by several span loadings designed to reduce wake velocities. Variations in the span loading on the swept-wing generator were obtained by deflecting seven flap segments on each side by amounts determined by vortex-lattice theory to approximate the desired span loadings. The resulting wakes were probed with a three-component, hot-wire probe to measure velocity, and with a wing to measure the rolling moment that would be induced on a following aircraft. The experimental techniques are described herein, and the measured velocity and rolling moments are presented, along with some comparisons with the applicable theories.

INTRODUCTION

The lift-generated vortices behind heavy aircraft present a hazard to smaller aircraft that might enter the region occupied by these vortices. The hazard may take the form of an overpowering rolling moment on the encountering aircraft or of large vertical accelerations or both. To understand better the hazard and possibly to reduce its magnitude, a theoretical and experimental study is being conducted to determine the structure, rate of decay, and means for modifying the vortices produced by a variety of lifting configurations. This research, conducted at NASA Ames Research Center, began by measuring the structure of the trailing vortices shed by a rectangular wing (refs. 1 through 6) and several swept-wing models (refs. 7 through 10). Measurements were made with a three-component, hot-wire probe and with a laser velocimeter. In the earlier tests (refs. 1 and 2), the wake was surveyed by holding the hot-wire probe in a fixed position during a measurement. The velocity determined by a fixed probe was then a time-averaged value at a particular location, which ignored the meandering motion of the vortex due to eddies in the wind-tunnel air stream. Since the meandering motion of the vortex can be of the order of the vortex core diameter or larger, the velocity distribution found by a fixed probe may be in appreciable error wherever large velocity gradients occur.

To eliminate the effects of vortex meander on the measured velocity profile, the hot-wire probe was mounted on the end of an arm of large radius

*Ames Research Center, NASA, Moffett Field Calif. 94035
**Nielsen Engineering & Research, Inc., Mt. View, Calif. 94043
***U. S. Army Air Mobility R&D Laboratory, Ames Research Center, Moffett Field, Calif. 94035

that rotated rapidly enough so that the circumferential velocity was large relative to the meander velocity (ref. 6). The rapid traverse of the probe through the vortex yielded a nearly instantaneous measurement of the vortex structure. This rotating-arm technique was first demonstrated by Corsiglia *et al.* (ref. 6) by investigating the vortices that trailed from two rectangular wings.

A laser velocimeter (LV), developed at about the same time at NASA/ARC (ref. 11), was also used to study the wakes of several wings (refs. 4, 5, and 7 through 10). The velocity data obtained with the rotating-arm, hot-wire apparatus in the wind tunnel agreed with that obtained with the rapid-scanning LV in the water tow tank. Further, the data yielded an understanding of the structure and decay process of lift-generated vortices that made it possible to correlate vortex data and thereby predict the vortex structure for large distances, not only behind the models tested in ground-based facilities but also behind full-scale aircraft (refs. 12 through 14).

A theoretical effort in support of the experimental program provided a simplification and improvement (ref. 15) of the Betz theory (ref. 16), which predicts the inviscid structure of fully developed vortices from the span loading on the wing. This theoretical tool was extended further by using the same conservation relationships for vortex systems to derive an inverse-rollup theory (ref. 17). The inverse method used measured data for the circumferential velocity in vortices to predict the span loading on the generating wing. The loadings predicted by the inverse-rollup theory agreed with those predicted by the vortex-lattice method of Hough (ref. 18), which is used when viscous and flow separation effects are small.

Some theoretical guidance (ref. 19) for alleviating the hazard presented by wake vortices was found by postulating a vortex wake that would not roll up from its edge but would remain flat. The properties of these vortex wakes and their possible applications to aircraft span loadings were then studied theoretically to determine if the concepts could be applied to aircraft. Significant reductions in the wake hazard were predicted in certain cases, but ground-based experiments were needed to determine whether the hypothetical loadings were effective and whether they could be utilized without prohibitive penalties.

The tests described in this paper were made to obtain data on the structure of vortices that trailed from the swept wing of a typical subsonic aircraft. A second objective was to obtain data on wings whose loadings approximated the unconventional span loadings that were predicted (in ref. 19) to reduce wake velocities. The model swept wing used in these tests was therefore equipped on each side with seven segmented flaps that could be deflected separately in 5° increments. The wakes of these configurations were probed with both the three-component, hot-wire probe and with a wing to measure the rolling moment induced on a following aircraft by the vortex wake. The technique used to obtain rolling moment parallels that of refs. 20 through 23. The data obtained on the vortex wakes with those two probe systems are presented here and compared with several theoretically predicted results.

2

APPARATUS AND TEST PROCEDURE

Wind-Tunnel Setup

As mentioned in the Introduction, two measurements were made in the wake of the generating wing: the velocity distribution for various flap configurations was measured using the experimental setup shown in figure 1; the rolling moment was measured using the setup shown in figure 2. In both cases, the wing used to generate the wake was located at the forward end of the test section and the hot-wire (or follower model) apparatus was at the exit of the test section of the NASA Ames Research Center 40- by 80-Foot Wind Tunnel. The wing used to generate the wake was centrally located in the inlet and was attached to a single strut through a strain-gage balance to measure lift. The planform of the swept wing and the flap settings are presented in figure 3a. The seven flap segments on each side were designed so that each could be replaced with a similar segment, but deflected a different amount. In this way, each flap could be changed in 5° increments to achieve span loadings that were, for convenience, called as follows: flaps 0°, landing, tailored, parabolic, and sawtooth. The flaps 0° configuration corresponded to the cruise settings; the landing settings approximated what could be used on swept wings for high lift during landing. The remaining three loadings were approximations to the hypothetical loadings studied theoretically in reference 19. These loadings were designed to produce large vortex cores (tailored and parabolic) or to generate multiple vortex wakes that would disperse quickly (sawtooth).

A vertical flatplate 0.02 b_g wide by 0.04 b_g high was used as a wing-tip spoiler on flaps 0° and landing configurations. As an extension of the studies in references 2 through 6, these tests were also to determine how the vortex wake would be modified by the introduction of turbulence. The spoiler was attached to the upper surface of the wing on the quarter-chord line, 0.10 b_g inboard from the tip and facing normal to the airstream.

Also presented here are some results for a wing whose planform was shaped or tailored (as described in reference 19 and shown in figure 3b) to yield large vortex cores. Only a limited amount of data were taken with this second wing to supplement the swept-wing investigation of tailored loading.

At a distance of 24.4 m (80 ft) downstream of the generator model, either the follower model or the hot-wire apparatus was mounted on a tower that could be positioned horizontally over a 4.27 m (14 ft) range. In addition, the follower model could be positioned vertically over a 3 m (10 ft) range. Additional details of the wings used to probe the wake (follower models) are given in figure 2. The only encounter direction studied was an axial penetration and the follower wing was held at zero incidence in all cases.

Most of the tests were conducted at a free-stream velocity of 40 m/s (q = 20.1 lb/ft^2) corresponding to a Reynolds number of 843,000 based on average wing chord. Several different values of free-stream velocity were used during the rolling-moment tests to obtain moments of a magnitude such that the optimum sensitivity of the balance could be used.

Velocity Measurement

As indicated in figure 1a, the three-component, hot-wire probe was fitted to the end of the arm having a radius of 2.24 m (7.34 ft) and was set at an angle so that it was aligned with the relative flow when the arm rotated at about 120 rpm. Hot-wire signals were carried through slip rings to the anemometer electronics located outside of the wind tunnel. This output and a time-code signal are then recorded on the following: magnetic tape for data reduction on a digital computer; paper chart for online editing and monitoring; and digital voltmeters to record dc signal levels. Further details on the instrumentation, calibration, and run procedure are contained in reference 3. A calibration air jet had been added to the apparatus since the tests described in reference 3 had been conducted. This jet impinged on the probe at the bottom of the arc of the rotating arm so that a signal from the jet was received on each revolution (figs. 1a and 4). Hot-wire anemometer data from the air jet was processed along with the vortex data. The air-jet results provided the following: an index to determine the azimuth angle of the arm at which the vortex was encountered by the probe; a measure of rpm; and a check of the calibration and time response of the hot-wire gear.

The test procedure consisted of moving the tower that supported the rotor arm assembly across the wind tunnel until, as noted on the paper-chart recorder, a maximum occurred in the number of vortices encountered per unit time by the hot-wire probe. A permanent record lasting about 5 min was then made on magnetic tape and paper chart. The paper-chart record was then used to select vortex encounters for analysis.

Rolling-Moment Measurement

The follower models were attached to the movable strut through a strain-gage balance to measure rolling moment or torque. The full-scale range for this balance was 11.3 Nm (100 in./lb), which provided adequate sensitivity for the rolling moments encountered. The follower models were constructed of balsa wood to ensure a high-frequency response to the imposed torques. The natural frequency of the model and balance combination was several times larger than the frequency content of the measured rolling-moment. As indicated in figure 2, three wings were used as the follower model. All had the same chord length and airfoil section, but a different span. This made it possible to study the effect on rolling moment of the span ratio of the follower to the generator.

The procedure for recording the rolling moment consisted of setting the generator-wing and wind-tunnel conditions and selecting a lateral and vertical position for the follower model. The time-varying signal was recorded on a light-beam, strip-chart recorder. Sufficient records were taken (usually about 1 min) to obtain the highest rolling moment for that location. The procedure was then repeated at successive lateral and vertical positions of the follower model in about 10 cm (4 in.) increments to determine the maximum value of rolling moment for the entire wake for each condition. Figure 5 shows a typical record of rolling-moment variation with time.

4

DATA REDUCTION PROCEDURE

Hot-Wire Signals

The procedure used by Corsiglia *et al.* (ref. 3) to reduce the analog data from the hot wires to velocity components has been modified and extended here to better accommodate the more diffuse vortices encountered in this investigation. A copy of a record of the hot-wire signals for one revolution of the rotor arm is presented in figure 6. The amplitude of a sine-wave signal taken at the beginning of a test period yielded the voltage-deflection relationship, which provided the calibrations for the velocity of the air as it passed the probe. The three-component, hot-wire signals were then used with these calibration values to calculate the three components of the velocity. The air-jet signals indicated where on the record the hot-wire probe passed near the bottom of its circle so that the azimuth angle of the vortex could be located. This information was then used with the nomenclature designated in figures 4 and 6 to relate the velocity data to the x, y, and z directions in the wind tunnel. For the data obtained in this test, the hot-wire records were hand faired from paper tape and then digitized for processing on an electronic computer. The processing was started by first finding the positions of the measured data relative to wind tunnel coordinates (fig. 6). The meandering motion of the vortex was removed from the cross-stream velocity components by subtracting the average of the velocity for each of the two components normal to the free-stream over the arc segment where data were analyzed; i.e., over $(S_{end} - S_{beg})$. The contribution to the velocity of the other vortex in the pair was also removed so that the data represented an isolated steady vortex. Since the corrections to the velocity for meander and for the other vortex were approximate, some scatter in the corrected data remained. When the velocity components had been corrected in this manner, the normals to the velocity vectors in the y-z plane were drawn to find the centers of the vortices, as illustrated in figure 7. The variations were then found of the circumferential and radial velocities as a function of radius from such a center. As shown in figure 8, each pass of the probe near or through a vortex yielded two values for the velocity components as a function of radius from the center of the vortex. That is, one set of data was obtained as the probe approached the vortex and one as it left the vortex. If the correct center for the vortex was chosen, the radial velocity was near zero, and the circumferential velocity was the same on approach and departure of the probe from the center of the vortex. The magnitude of the radial component of velocity and the asymmetry of the vortex indicated the accuracy of the results. The vortex centers were chosen to reduce the magnitude of these quantities.

The foregoing process was carried out for five passes of the rotor arm through the vortex wake of the configuration being tested. A faired and averaged curve was constructed from these data points and was then used as the velocity distribution in the vortex trailed by the particular configuration.

5

Rolling Moment

As mentioned previously, the rolling moment was measured on a model wing as it was held at various locations in the wake generated by the swept-wing model. The maximum rolling moment observed for each configuration was converted to a rolling-moment coefficient, defined as

$$C_{l_f} = \frac{\text{rolling moment}}{q S_f b_f}$$

where $q = \frac{1}{2} \rho U_\infty^2$ is the dynamic pressure, S_f and b_f are (respectively) the wing planform area and span of the follower model. As indicated in figure 5, the peaks were often repeated several times during a run to confirm that the maximum value was not a rare occurrence. The probe was usually held in one location for about 1 min. When single peaks were much higher than the rest of the data, they usually happened near the fringe of the wakes and were interpreted as extreme excursions in the meander of the vortex.

DISCUSSION OF RESULTS

Vortex Velocity Data and Comparison with Rollup Theories

The hot-wire measurements made in the wakes of the various wing and flap configurations shown in figure 3 and discussed previously were reduced to axial and circumferential velocity components using the foregoing procedure. Figure 9 presents the averaged curves for the measured circumferential velocity in the vortices shed by the various swept-wing configurations and by the tailored-planform wing. The data were normalized by the lift coefficient on the generating wing to remove lift as a variable in the comparison. It is noted in figure 9 that some variation in the maximum circumferential velocity and the radius at which it occurs (i.e., the core radius of vortex) exists between the various configurations tested (see fig. 3). As expected, the vortex with the largest core was produced by the swept wing with the flaps deflected to produce a tailored loading. No averaged curve was found to represent the circumferential velocity in the vortex wake shed by sawtooth loading. Since each pass of the hot-wire probe through the wake yielded a different velocity profile with several possible vortex centers, the wake was believed to consist of several vortex pairs so that the wake could not be correctly represented by a single vortex pair.

The measured streamwise component of the velocity usually differed from the free-stream velocity only in the vortex core — and then, at most, by about 10%. The following analysis of rolling moment assumed that the streamwise component (or x component) of the velocity was equal to the free-stream velocity.

Vortex velocities, direct-rollup theory — A theoretical tool frequently used to study the circumferential velocity distribution in lift-generated

6

vortices is the simple rollup method of Betz (ref. 16). His theory is based on the conservation equations for inviscid, two-dimensional vortices and relates the circulation in the fully developed vortex to the span loading on the generating wing. The simplicity of the method results from the assumptions that the vortex is completely rolled up and that the rollup process is inviscid. To achieve a unique result, the vortex sheet is assumed to roll up in an orderly fashion inboard, from the wing tip, so that successive layers of the sheet are wrapped around and over the center of previous wrappings (fig. 10). Any axial or streamwise variation in the flow velocity is assumed to have a negligible effect on the rollup process. The Betz method does not treat the transition or intermediate stages between the initial vortex sheet behind the wing and the final rolled-up vortex structure. By this technique, the vortex structure is related to the span loading on the generating wing by (e.g., ref. 15),

$$\Gamma_w(y_1) = \Gamma_v(r_1) = 2\Pi r v_\theta \tag{1}$$

where the radius in the vortex r_1 is related to a spanwise station on the wing y_1 by

$$r_1 = -\frac{1}{\Gamma_w(y_1)} \int_{b/2}^{y_1} \Gamma_w(y) \, dy \tag{2}$$

The symbol Γ_w denotes the bound circulation on the wing, and Γ_v the circulation in the fully developed vortex.

Since the data in figure 9 have the contribution of the companion vortex removed, the vortex is axially symmetric and represents the vortex shed by an isolated wingtip. It can therefore be compared with the velocity distribution predicted by equations (1) and (2) by using the span loadings predicted for the generating wing by vortex-lattice theory (ref. 18). The span loadings predicted for the various swept-wing configurations using this inviscid method are shown in figure 11 at the angle of attack for which the hot-wire data were taken. The measured velocity data are compared in figure 12 with the predicted velocities from equations (1) and (2) and the span loadings in figure 11. As expected, the agreement is quite good in the outer parts of the vortex. The differences that sometimes occur near the vortex center are attributed to the choice of how the vortex sheet shed by the wing was assumed to roll up. If a different rollup sequence had been assumed, the agreement could sometimes be improved. For example, in the landing configuration, the theory should assume two vortices instead of one. Two vortices formed near the wing but the flow visualization with smoke indicated that these two merged before they reached the measuring station in the wind tunnel. The Betz theory used to predict the vortex structure in figure 12 does not account for vortex merging. Also, the method does not account for the boundary layer on the wing that enters the core region near the center of the vortex. The comparison indicates that the direct-rollup theory is adequate for many purposes, because the predictions are quite accurate for the outer part of the vortex, even though they are not always reliable near the center.

Span loading, inverse-rollup theory — The measured vortex structure is used here to predict the span loading on the generating wing by means of an inverse-rollup theory (ref. 17). This backward moving process is based on the same basic equations and assumptions as the direct Betz method. The derivation is begun with the expression presented previously, which relates the radius r_1 in the vortex to the spanwise station on the wing y_1, which contains a given amount of circulation. After some simple manipulations and, because the vortex is axially symmetric so that the circulation may be written as $\Gamma_v = 2\pi r_1 v_\theta$, the inverse relationship becomes

$$\frac{b}{2} - y_1 = r_1 + \int_0^{r_1} \frac{d(rv_\theta)}{v_\theta} \tag{3}$$

where v_θ is the measured circumferential velocity in the vortex.

Figure 13 compares the span loadings predicted by vortex-lattice theory with those predicted by the inverse-rollup theory. These comparisons were made by adjusting the span loading calculated by the vortex-lattice theory so that the area under the span loading curve is the same as that predicted by the inverse-rollup method. The results in figure 13 show that the inverse rollup theory can recover the span loading on the generating wing fairly accurately. With almost all configurations, a difference occurs near the wing tip as a result of the finite core size and solid-body rotation in the vortex near $r = 0$. The magnitude of the distortion in span loading depends on the size of the core, which is influenced by the character of the boundary layer on the wing and on the viscous and turbulent shear forces in the vortex itself. In most cases, these distortions appear to be small and to occur near the wing tip only.

The agreement between theory and experiment found for the inverse-rollup method is better, in some cases, than for the direct-rollup method. It is believed that this is caused by the difference in the integration process, which tends to suppress inaccuracies for small radii for the inverse-rollup theory and to amplify them in the direct-rollup theory. This is best seen by noting in equation (3) that the velocity variation in the vortex is multiplied by the radius, which tends to suppress inaccuracies. Equation (2), however, for the direct-rollup calculations has small values of $\Gamma_w(y_1)$ when near the vortex center (i.e., $y_1 \leq b/2$) so that inaccuracies are amplified. In the direct-rollup method, these differences are suppressed at large radii. Contrarily, the inverse-rollup method, which is insensitive to inaccuracies at small radii, accumulates errors so that the largest deviations from theory are found near the wing centerline (i.e., as if from the outer radii of the vortex). However, if these limitations of the rollup methods are kept in mind, the rollup methods can provide useful relationships between the span loading on the generating wing and the vortex structure.

Region of applicability of rollup theories — The simplicity of both the direct and inverse rollup methods results from the assumptions that the vortex is completely rolled up and that the rollup process is inviscid. These two assumptions then limit the downstream interval over which the theories apply.

8

The upstream end of the region of applicability begins where the rollup of the vortex sheet is largely completed and can be estimated by use of inviscid, time-dependent rollup calculations. Results such as those in figures 6 and 10 of Rossow (ref. 24) indicate that a major part of the rollup process behind many wings can be considered as practically complete within three to five span lengths behind the generating wing.

The downstream end of the region of applicability is the distance at which viscous and turbulent decay of the vortex has modified its structure to the extent that the inviscid theory no longer approximates it. An estimate for this limit can be obtained from the recent data of Ciffone and Orloff (ref. 9) wherein a so-called plateau region (to be discussed in the next section) is identified. Within this plateau region, they found that the vortex decays very little, but is followed by a region where the vortex decays roughly as $t^{-1/2}$. These considerations suggest that the region of applicability of the Betz method lies between about three span lengths and the downstream end of the plateau region.

Rolling Moment on Following Wing

Experimental data — As mentioned in the foregoing text, the rolling moment on a follower wing was measured at a variety of locations in the wake produced by the various configurations of the swept-wing generator. The maximum rolling moments experienced by the three follower wings described in the table in figure 2 are presented in figure 14. The quantity C_{l_f}/C_{L_g} was used because it permitted comparison of the various configurations at the same lift. This parameter would theoretically be a constant if the span loading did not change with the angle of attack. However, the flap settings used in the present test cause some changes in the span loading as the angle of attack changes, so that the data in figure 14 are, in most cases, a function of C_{L_g}. Note that aircraft typically have the control capability to create a rolling-moment coefficient of 0.04 to 0.06. Hence, any imposed torque by a vortex that causes C_{l_f} to exceed about 0.06 will cause the encountering aircraft to roll even when full counter-roll control is imposed.

Several of the results in figure 14 are of particular interest. First, the tailored loading is noted to have higher values of C_{l_f}/C_{L_g}. A theoretical estimate (ref. 24) of the torque to be expected on a model when it encounters the wake of a swept wing with tailored loading indicated that the torque would be less than for elliptic loading only if the span of the follower wing were less than about 20% of the tailored portion of the generating wing. Since all but the smallest of the following models tested had a span larger than 20% of the generating wing, it was expected that the rolling moment induced on all of them would be larger than for the flaps 0° configuration. For the smallest follower, it was found that sawtooth loading or the addition of a spoiler to the flap 0° configuration were both more effective than tailoring the wing (see fig. 14a).

Another result that is of special interest is the rolling moment measured on the smallest following wing in the wake of the swept wing configured

to develop sawtooth loading (see fig. 14a). The generation of multiple vortices in the wake appears to be quite effective, in that case, for reducing the rolling moment at low lift coefficients. However, the effectiveness disappears as the lift increases above $C_{L_g} = 0.4$. Some alleviation was also achieved on the larger follower $(b_f/b_g = 0.29)$ with sawtooth loading, but not to the extent realized with the smallest follower.

A 2-ft span version of the swept wing was tested by Ciffone and Orloff (ref. 9) by towing the wing through a water tank. Their tests showed that the vortices shed by the sawtooth loading at $C_{L_g} = 0.7$ undergo large excursions in the wake which are of the order of one-half the span of the generator and that the various pairs execute destructive interactions which tend to disperse the wake vorticity. But when the various vortex motions in the sawtooth wake were finished, a single vortex pair still remained, indicating that the vorticity had not been completely dispersed. These preliminary results in the wind tunnel and in the water tow tank indicate that, as predicted in reference 19, large excursions in the wake can be produced by multiple vortex pairs, but that additional guidelines are needed to design the sawtooth loading so that the dispersion of vorticity will be complete.

Predicted rolling moment — The theoretical estimate of the rolling moment is restricted to an axial penetration of the wake by the following wing. Extension of the method to other types of encounters (e.g., where the vortex is crossed at about 90° to its axis) may require the inclusion of nonsteady loading effects. Penetrations that deviate only slightly from axial are usually assumed to be approximated quite well by steady-state flow theories. Figure 15 presents a schematic of the flow field for an encounter wherein the vortex and wing centerlines are aligned. The axial or streamwise velocity is assumed equal to the free-stream velocity. The circumferential velocity in the vortex used as the up- or downwash on the follower wing is obtained from the measurements presented in figure 9 by adding the contributions of both the left and right vortices in the wake. The torque or rolling moment on an encountering wing has been calculated by a variety of theories, which are:

1. Two-dimensional strip theory
2. Strip theory with empirical lift-curve slope correction.
3. Vortex-lattice theory; flat-wake approximation.

The two-dimensional strip theory for the rolling moment assumes that the lift on each spanwise wing element is given by its two-dimensional value, or,

$$\ell(y) = C_{L_\alpha} \sin \alpha \, \tfrac{1}{2} \rho \, U_\infty^2 \, c(y) \tag{4}$$

where C_{L_α} is the two-dimensional lift-curve slope of the airfoil section at that spanwise station, $\sin \alpha \approx w/U_\infty$ is the flow inclination, and $c(y)$ is the local chord of the wing. When the quantity $y\ell(y)$ is integrated across the span of the rectangular wings used in this study, the rolling-moment coefficient becomes

$$C_{l_f} = \frac{C_{L_\alpha}}{b_f^2} \int_{-b_f/2}^{b_f/2} (w/U_\infty) y \, dy \tag{5}$$

The values presented in table 1 were found by integrating equation (5) numerically after setting $\frac{w}{U_\infty}$ equal to the sum of the measured $\frac{v_\theta}{U_\infty}$ contributions of the left- and right-side vortices. A different form of equation (4) can be obtained when only one vortex is acting on the following wing by setting $\frac{w}{U_\infty} = \frac{v_\theta}{U_\infty} = \frac{\Gamma(r)}{2\pi r U_\infty}$ and letting $y = r$.

$$C_{l_f} = 2 \left(\frac{C_{L_\alpha}}{2\pi}\right)\left(\frac{b_g}{b_f}\right)^2 \int_0^{\frac{b_f}{2b_g}} \left[\frac{\Gamma(r)}{b_g U_\infty}\right] d\left(\frac{r}{b_g}\right) \tag{6}$$

Although equation (6) is sometimes more convenient, equation (5) is used here because it is believed to be more accurate for the wakes being considered.

For two-dimensional wings, the lift-curve slope, C_{L_α}, is usually taken as 2π. As noted in table 1, the predictions made with equation (5) are then generally too high because it does not account for the induced angles of attack near the wingtips and near the vortex centerline. An empirical relationship for the lift-curve slope to be used in the calculation of torque may be obtained by use of the formula introduced by R. T. Jones (page 95 of ref. 25):

$$C_{L_\alpha} = \frac{2\pi R}{P \cdot R + 2} \tag{7}$$

where R = aspect ratio and P = semiperimeter/span. Maskew* compared the rolling moment calculated by vortex-lattice theory and of the strip theory with several versions of equation (7). He concluded that the span, aspect ratio, and perimeter in equation (7) should be interpreted on the basis of one-half of a wing when the vortex and wing center are aligned. He reasoned that each half of the wing then acts as a separate wing, and equation (7) should be interpreted accordingly. For the rectangular wings studied here, equation (7) then becomes

$$C_{L_\alpha} = \frac{2\pi AR_f}{R_f + 6} \tag{8}$$

The strip-theory predictions corrected for C_{L_α} by equation (8) are noted in table 1 to be in good agreement with the vortex-lattice theory and in fair agreement with experiment. The vortex-lattice theory used is a version of

*B. Maskew, Hawker Siddeley Aviation, Ltd. (presently NRC Associate at Ames Research Center), private communication.

11

Hough's (ref. 18) and of Maskew's (ref. 26) methods adapted to the present situations. The differences that occur between the vortex-lattice theory and experiment may be due to any of the following: differences in the interpretation of the measured rolling moments; differences in the vortex velocity data; a combination of both; or unsteady aspects of the wind tunnel measurements, which were assumed negligible. Nevertheless, the foregoing results indicate that either the vortex-lattice theory or the simple strip theory with C_{L_α} determined by the Jones-Maskew formula provides reasonable estimates for for the rolling moment induced by a vortex on a follower wing.

With the empirically adjusted strip theory, the rolling moment and lift on a wing can be simply calculated at a large number of points in the wake. Contours of equal rolling moment coefficient and lift interpolated from these points are presented in figure 16 for one vortex and one span ratio. Only one quadrant is presented because the flow field is symmetrical vertically and antisymmetrical about the centerplane. Although the contours are not as precise as if determined by vortex-lattice theory, they do indicate the nature of the area over which high values of rolling moment occur. As expected, the maximum rolling moment occurs when the encountering wing is centered on the vortex. The shaded area in figure 16a within the contour labeled 0.06 can be interpreted, for example, as a hazardous region where overpowering rolling moments are to be found. Similarly, the results in figure 16b indicate that large values of positive and negative lift are induced on the follower by the vortex wake depending on its location relative to the vortex pair. As expected, the shape of the curves of constant torque and lift change with both the vortex structure and with the span of the follower.

CONCLUDING REMARKS

The experiments conducted with the flaps deflected to produce various span load distributions on a model swept wing show that the wake structure is affected by the shape of the span loading on the generating wing. The tailored and sawtooth span loadings tested indicate that the predicted characteristics of the wake were achieved but that the alleviation of the rolling moment on a follower wing was not as much as needed (e.g., $C_{l_f} \leq 0.06$). Further improvement with tailored loading is probably not to be expected because the enlargement of the vortex core that can be readily obtained does not have a profound reduction in rolling moment. Sawtooth loading did cause large excursions in the wake and did bring about a substantial reduction in rolling moment in a limited region of applicability. Additional criteria are therefore needed to define better the shape of the sawtooth loading so that wake alleviation can be achieved over a wide variety of conditions.

Comparison of the vortex structure and span loadings with rollup theories indicates that they are fairly reliable methods for studying vortex wake characteristics. Care must be taken, however, to be sure that the assumptions made in the theory are also satisfied in the experiment.

12

The fair agreement between measured torque and the vortex-lattice theoretical predictions suggests that the steady-state approximation is probably satisfactory for near-axial penetration of the vortex wake.

REFERENCES

1. Chigier, N. A.; and Corsiglia, V. R.: Tip Vortices—Velocity Distributions. NASA TM X-62,087, 1971. (Also presented at 17th Annual National Forum of the American Helicopter Society, May 1971).

2. Chigier, N. A.; and Corsiglia, V. R.: Wind-Tunnel Studies of Wing Wake Turbulence. J. of Aircraft, vol. 9, no. 12, 1972, pp. 820-825.

3. Corsiglia, V. R.; Schwind, R. K.; and Chigier, N. A.: Rapid-Scanning Three-Dimensional Hot-Wire Anemometer Surveys of Wing-Tip Vortices. J. of Aircraft, vol. 10, no. 12, 1973, pp. 752-757.

4. Orloff, K. L.; and Grant, G. R.: The Application of a Scanning Laser Doppler Velocimeter to Trailing Vortex Definition and Alleviation. AIAA Paper 73-680, 1973.

5. Orloff, K. L.: Trailing Vortex Wind-Tunnel Diagnostics with a Laser Velocimeter. J. of Aircraft, vol. 11, no. 8, 1974, pp. 477-482.

6. Corsiglia, V. R.; Jacobsen, R. A.; and Chigier, N. A.: An Experimental Investigation of Trailing Vortices Behind a Wing With a Vortex Dissipator. Aircraft Wake Turbulence and Its Detection, edited by J. Olson, A. Goldberg, and M. Rogers, Plenum Press, New York, 1971, pp. 229-242.

7. Ciffone, D. L.; Orloff, K. L.; and Grant, G. R.: Laser Doppler Velocimeter Investigation of Trailing Vortices Behind a Semi-Span Swept Wing in a Landing Configuration. NASA TM X-62,294, 1973.

8. Orloff, K. L.; Ciffone, D. L.; and Lorincz, D.: Airfoil Wake Vortex Characteristics in the Far Field. NASA TM X-62,318, 1973.

9. Ciffone, D. L.; and Orloff, K. L.: Far Field Wake Vortex Characteristic of Wings. AIAA Paper No. 74-505, AIAA 7th Fluid and Plasma Dynamics Conference, Palo Alto, Calif., June 17-19, 1974.

10. Orloff, K. L.; and Ciffone, D. L.: Vortex Measurements Behind a Swept Wing Transport Model. J. of Aircraft, vol. 11, no. 6, 1974, pp. 362-364.

11. Grant, G. R.; and Orloff, K. L.: A Two-Color Dual-Beam Backscatter Laser Doppler Velocimeter. Applied Optics, vol. 12, 1973, p. 2913.

12. Ciffone, D. L.; and Orloff, K. L.: Axial Flow Measurements in Trailing Vortices. AIAA Journal, vol. 12, no. 8, 1974, pp. 1154-1155.

13. Ciffone, D. L.: Correlation for Estimating Vortex Rotational Velocity Downstream Dependence. J. of Aircraft, vol. 11, no. 11, 1974, pp. 716-717.

14. Iversen, J. D.: Correlation of Turbulent Trailing Vortex Decay Data. J. of Aircraft (to be published).

15. Rossow, V. J.: On the Inviscid Rolled Up Structure of Lift-Generated Vortices. J. of Aircraft, vol. 10, no. 11, 1973, pp. 647-650.

16. Betz, A.: Verhalten von Wirbelsystemen. Z.A.M.M., Bd. XII, Nr. 3, 1932, pp. 164-174 (see also NACA TM 713).

17. Rossow, V. J.: Prediction of Span Loading from Measured Wake-Vortex Structure — An Inverse Betz Method. J. of Aircraft (to be published).

18. Hough, G.: Remarks on Vortex-Lattice Methods. J. of Aircraft, vol. 10, no. 5, 1973, pp. 314-317.

19. Rossow, V. J.: Theoretical Study of Lift-Generated Vortex Sheets Designed to Avoid Rollup. NASA TM X-62,304, 1973.

20. Wentz, W. H. Jr.: Evaluation of Several Vortex Dissipators by Wind Tunnel Measurements of Vortex-Induced Upset Loads. Wichita State University Aeronautical Report 72-3, 1972.

21. Singh, B.; Kutty, T. M.; and Wentz, W. H. Jr.: Preliminary Investigation of Rolling Moments Induced by Trailing Vortices for Several Wing-Tip Modifications. Wichita State University Aeronautical Report 72-1, 1972.

22. Banta, A. J.: Effects of Planform and Mass Injection on Rolling Moments Induced by Trailing Vortices. Master's thesis, Wichita State University, Wichita, Kansas, 1973.

23. Iversen, J. D.; and Bernstein, S.: Trailing Vortex Effects on Following Aircraft. J. of Aircraft, vol. 11, no. 1, 1974, pp. 60-61.

24. Rossow, V. J.: Theoretical Study of Lift-Generated Wakes Designed to Avoid Rollup. AIAA J., vol. 13, no. 4, 1975, pp. 476-484.

25. Jones, R. T.; and Cohen D.: Aerodynamics of Wings at High Speeds. Aerodynamic Components of Aircraft at High Speeds, vol. VII, edited by A. F. Donovan and H. R. Lawrence, Princeton University Press, 1957.

26. Maskew, B.: Numerical Lifting Surface Methods for Calculating the Potential Flow About Wings and Wing-Bodies of Arbitrary Geometry. Ph.D. thesis, Loughborough University of Technology, 1972.

TABLE 1.— COMPARISON OF PREDICTED AND MEASURED ROLLING-MOMENT COEFFICIENTS.

Configuration	α	C_{L_g}	b_f/b_g	$\mathcal{R}_f$	Normalized rolling moment, C_{l_f}/C_{L_g}			
					Measured	Strip theory		Vortex-lattice theory
						$C_{L_\alpha} = 2\pi$	Empirical C_{L_α}	Flat-wake approximation
Flaps 0°	8°	0.75	0.29	5.84	0.092	0.222	0.110	0.109
Flaps 0° plus spoiler	8°	0.70	---	---	0.053	0.184	0.091	0.085
Landing	6°	0.85	---	---	0.081	0.243	0.120	0.117
Landing plus spoiler	8°	0.86	---	---	0.081	0.163	0.081	0.071
Tailored	10°	0.82	---	---	0.105	0.246	0.122	0.111
Flaps 0°	8°	0.75	0.14	2.82	0.099	0.317	0.101	0.090
Flaps 0° plus spoiler	8°	0.70	---	---	0.023	0.154	0.049	0.038
Tailored	10°	0.82	---	---	0.074	0.173	0.055	0.042

HOT WIRE PROBE

ROTATING ARM

INSTRUMENT TOWER

AIRJET

1.84

24.4

6.1

₵

DIMENSIONS IN m
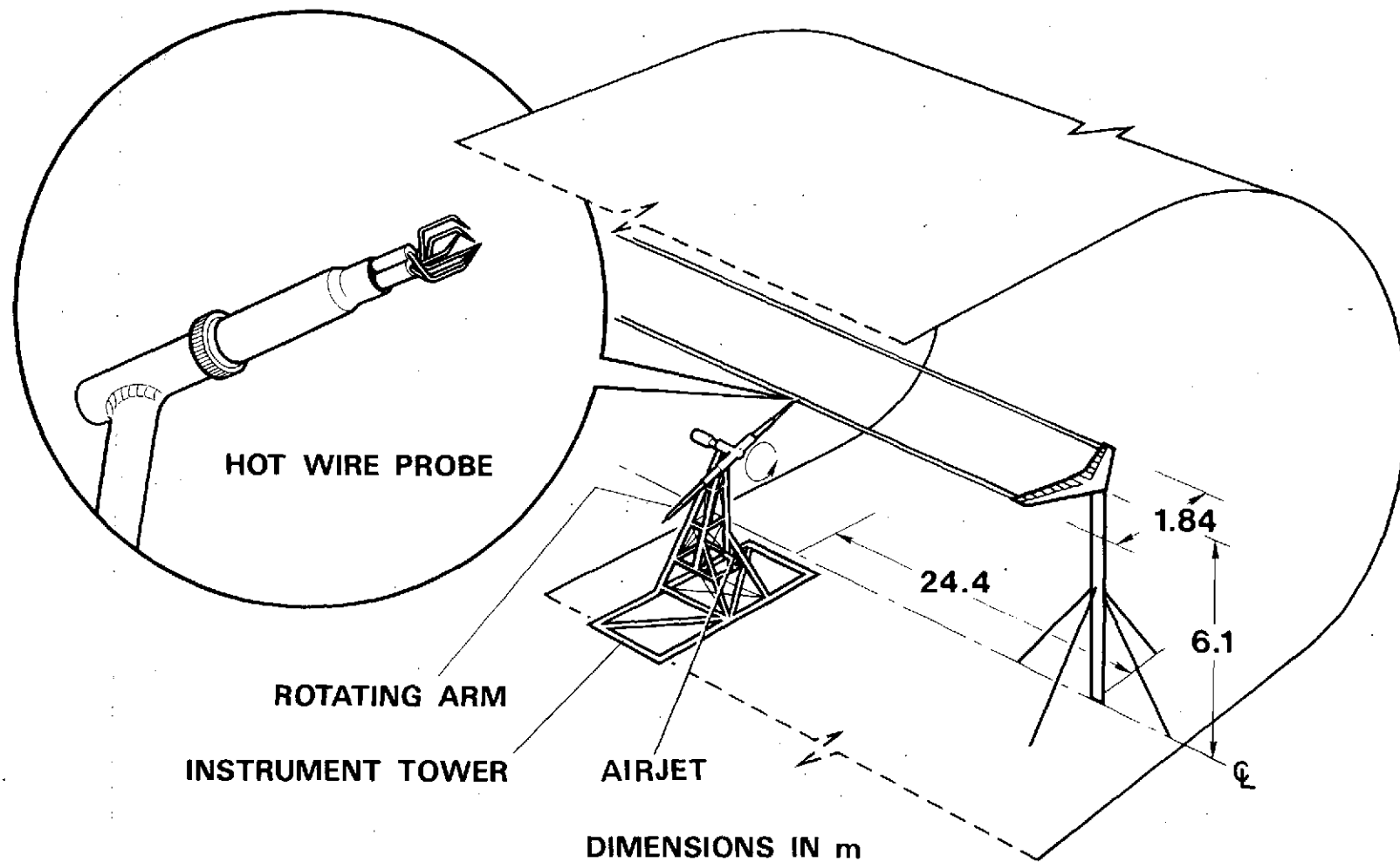
(a)   Schematic of setup.

Figure 1.— Technique used in 40- x 80-foot wind tunnel to measure the three
velocity components in the wake of the swept-wing model.

(b) Photograph of setup in wind tunnel.
Figure 1.— Concluded.

FOLLOWING MODELS			
b_f	c_f	R_f	b_f/b_g
26.4cm (10.4 in.)	9.02cm (3.55 in.)	2.93	0.14
52.7cm (20.8 in.)	9.02cm (3.55 in.)	5.84	0.29
91.4cm (36 in.)	9.02cm (3.55 in.)	10.14	0.50

1.84

24.4

6.1

INSTRUMENT TOWER

DIMENSIONS IN m
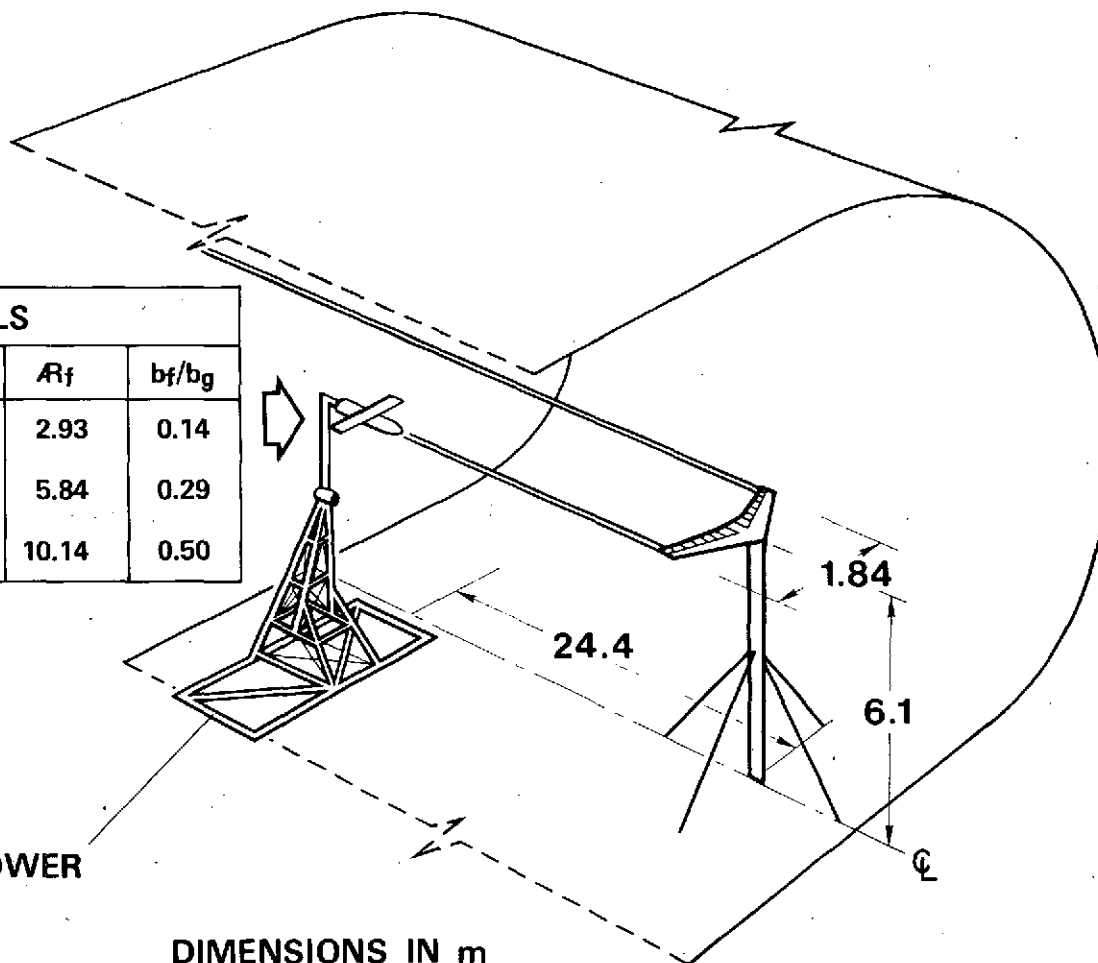
Figure 2.— Setup in the 40- by 80-foot wind tunnel used to measure the rolling moment on the model wing in the wake of a swept-wing model.
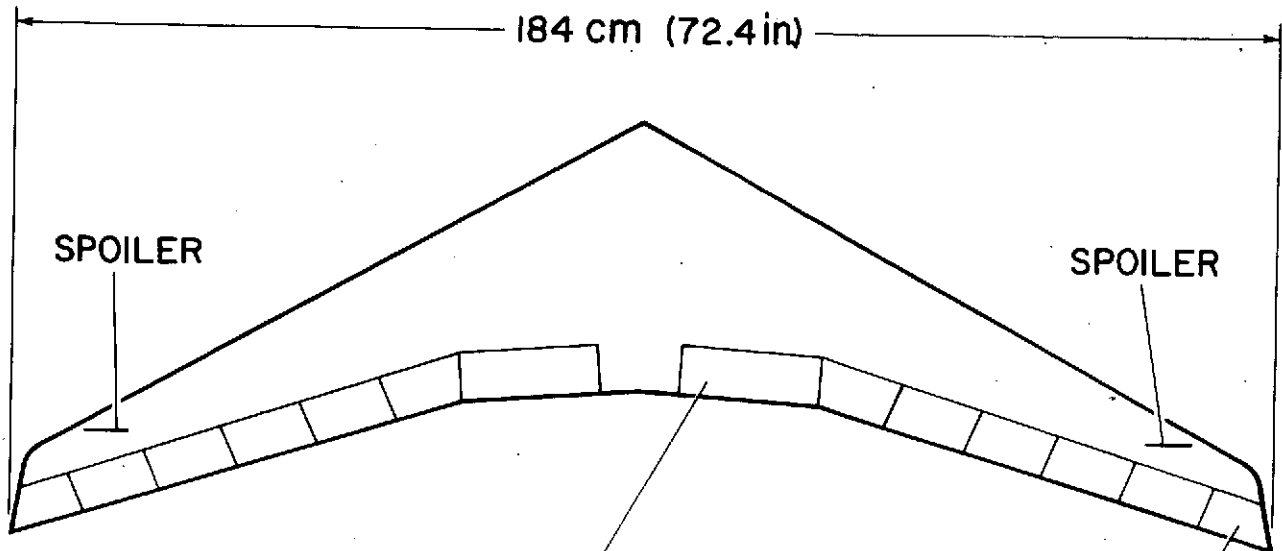
CONFIGURATION	FLAP SETTINGS						
	INBOARD						OUTBOARD
FLAPS 0°	0°	0°	0°	0°	0°	0°	0°
LANDING	20°	20°	20°	0°	0°	0°	0°
TAILORED	10°	10°	0°	−10°	−15°	−20°	−30°
PARABOLIC	10°	10°	10°	10°	0°	−10°	−20°
SAWTOOTH	−15°	15°	−15°	15°	−15°	15°	−15°

(a) Swept wing. Spoiler is 0.02 b_g wide by 0.04 b_g high.
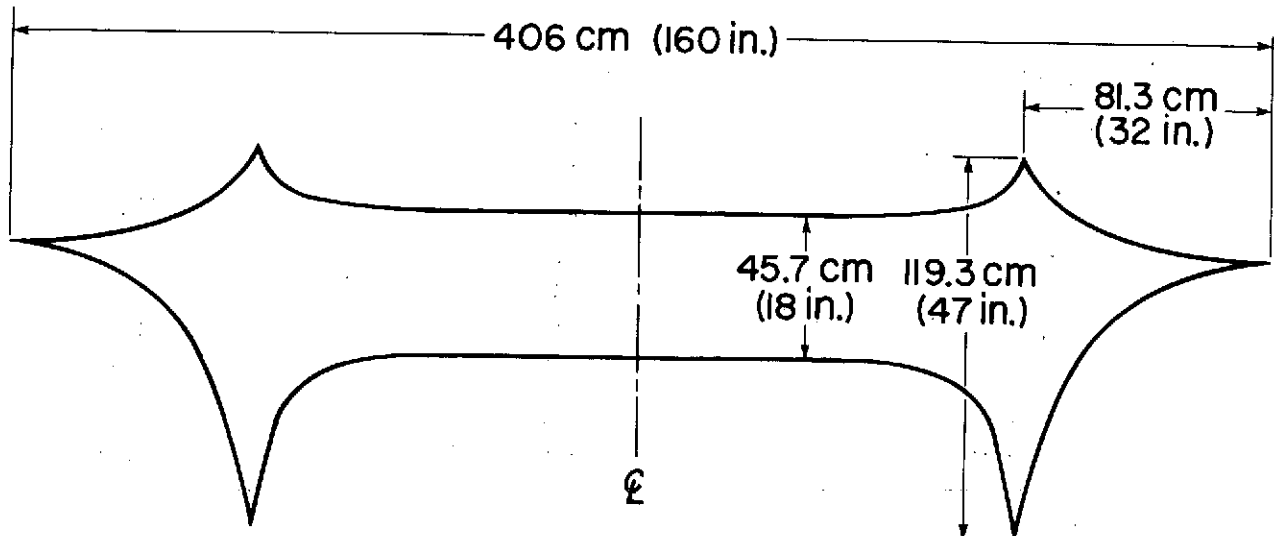
(b) Planform of an unswept wing tailored 40% of semispan (from ref. 19).

Figure 3.— Plan view of wings used to generate wakes.
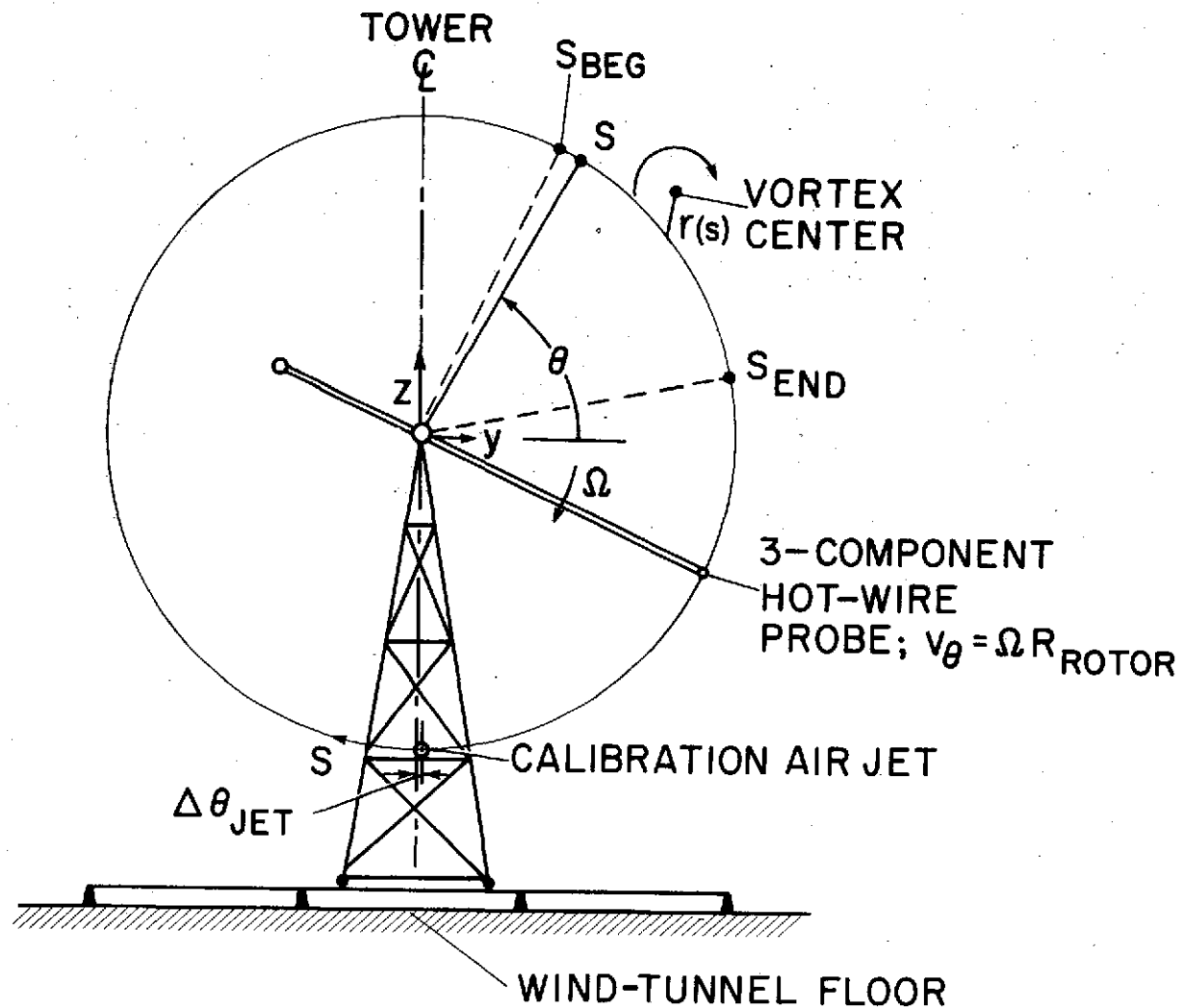
Figure 4.— Schematic diagram of rotor tower with nomenclature used to deduce velocity components from hot-wire measurements.
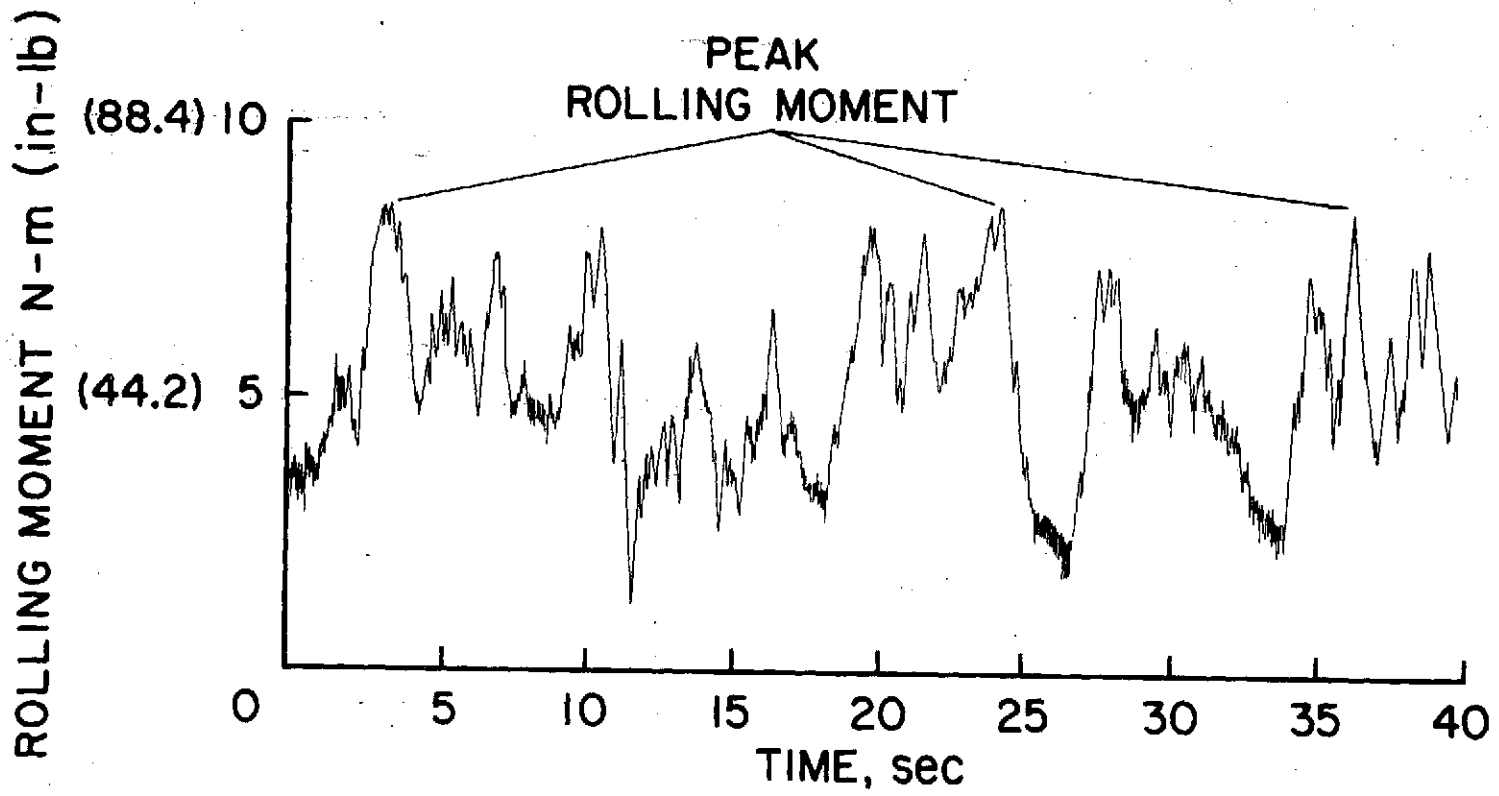
Figure 5.— Typical time-dependent record of rolling moment induced on the follower wing as it encounters the wake of the generating wing.
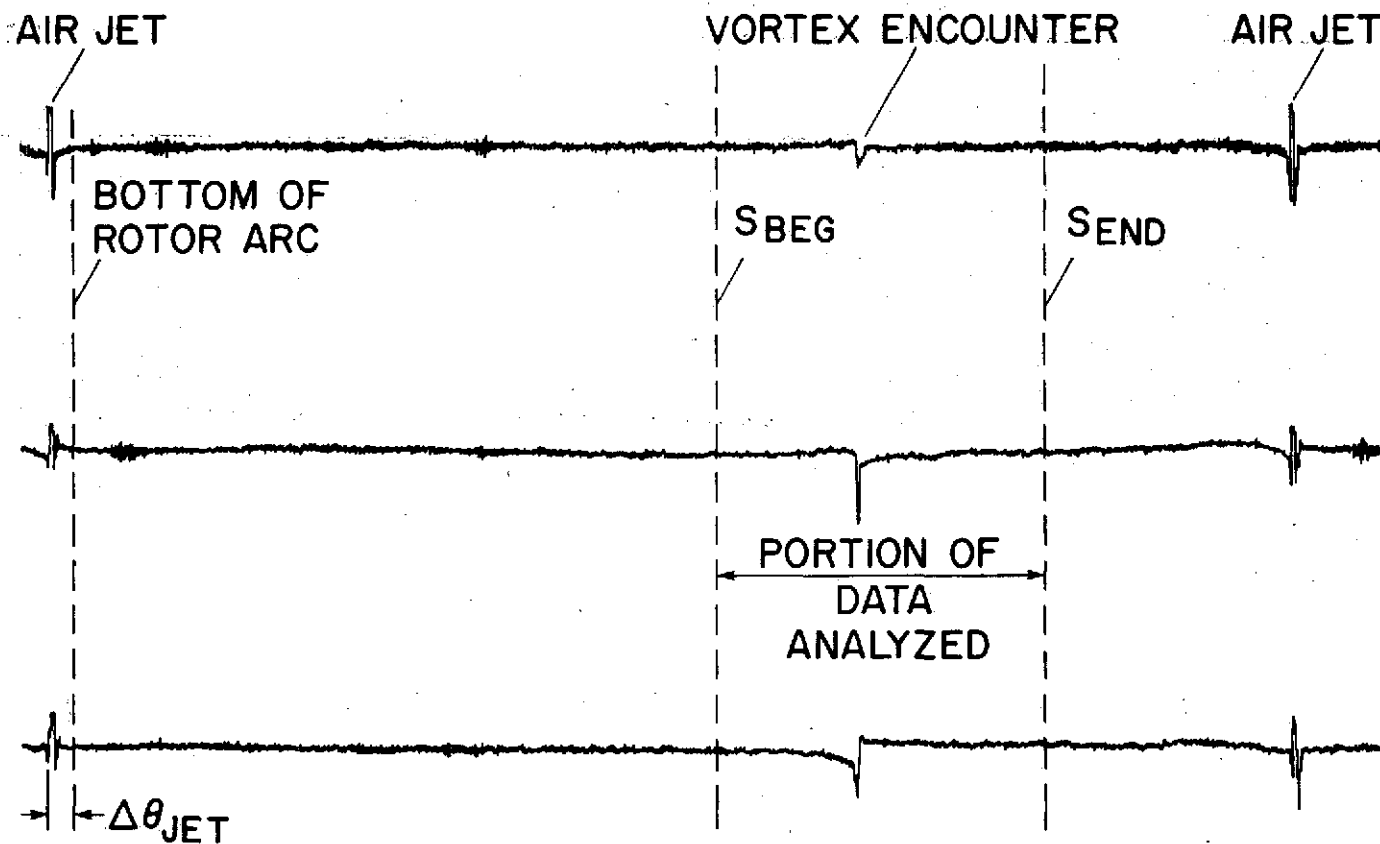
Figure 6.— Typical hot-wire signals for one rotation of the rotor arm through the wake of a swept-wing model; flaps 0°, $\alpha = 8°$.
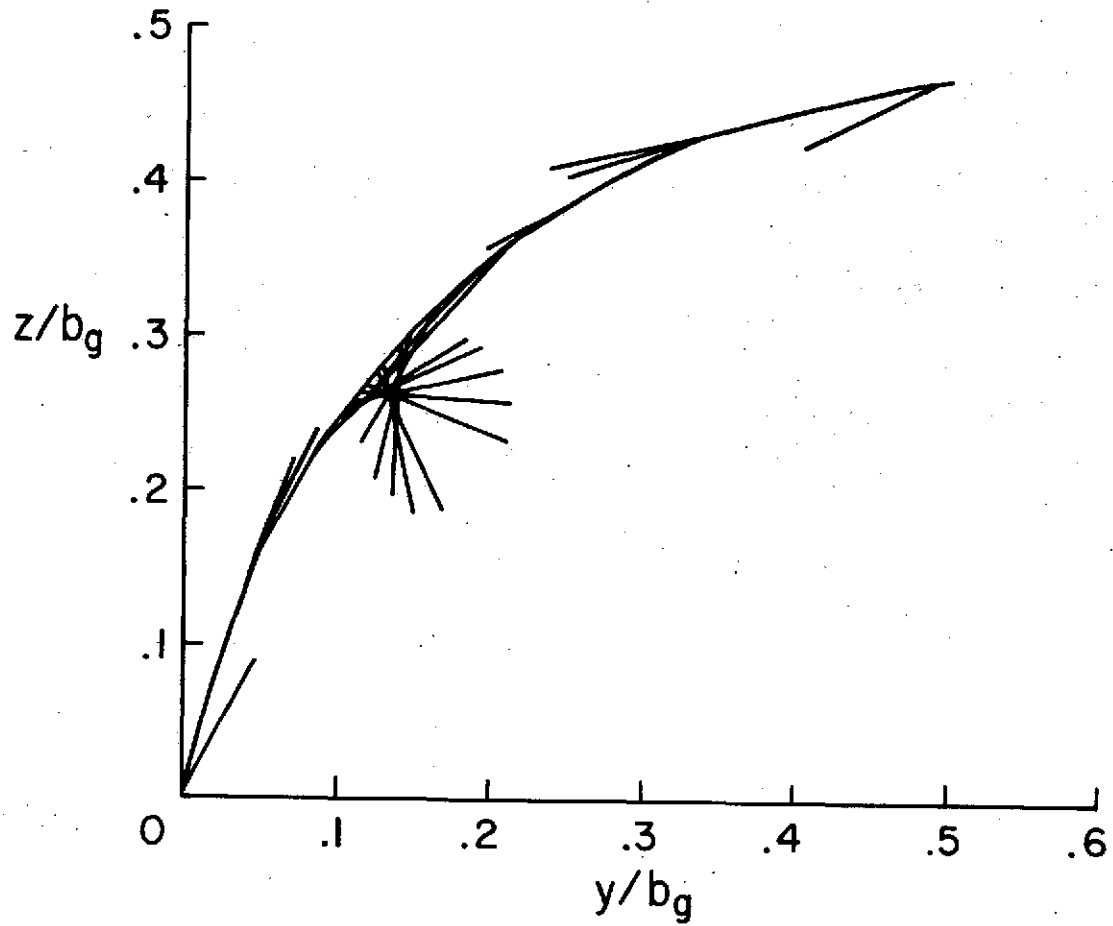
Figure 7.— Example of the vectors drawn perpendicularly to the velocity vectors in the plane of the rotor to locate the centers of the vortices in the wake; wing planform tailored 40%, $\alpha = 12°$, $C_L = 0.85$.
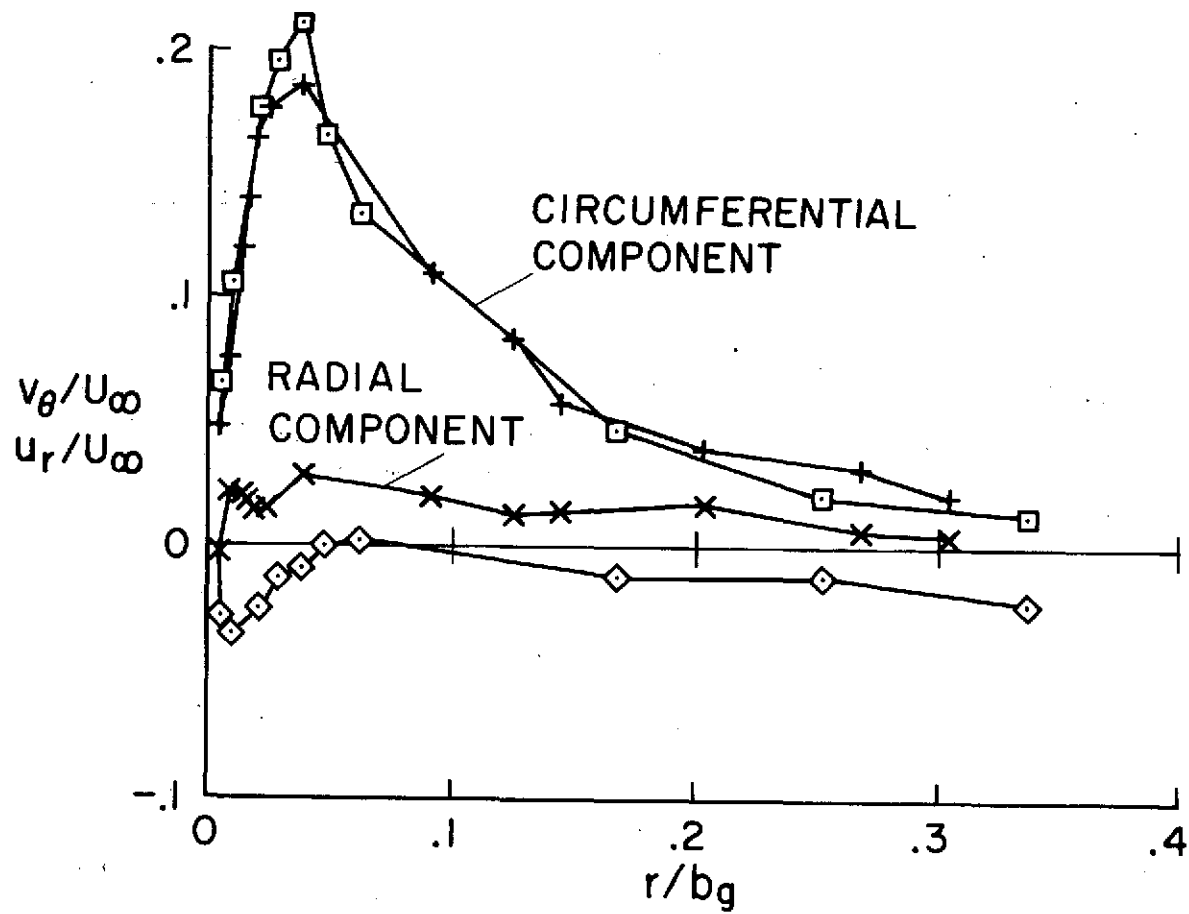
Figure 8.— Example of the variation of radial and circumferential velocity components with the radius from the center of the vortex for data along the arc of the rotor; wing planform tailored 40%, $\alpha = 12°$, $C_L = 0.85$.
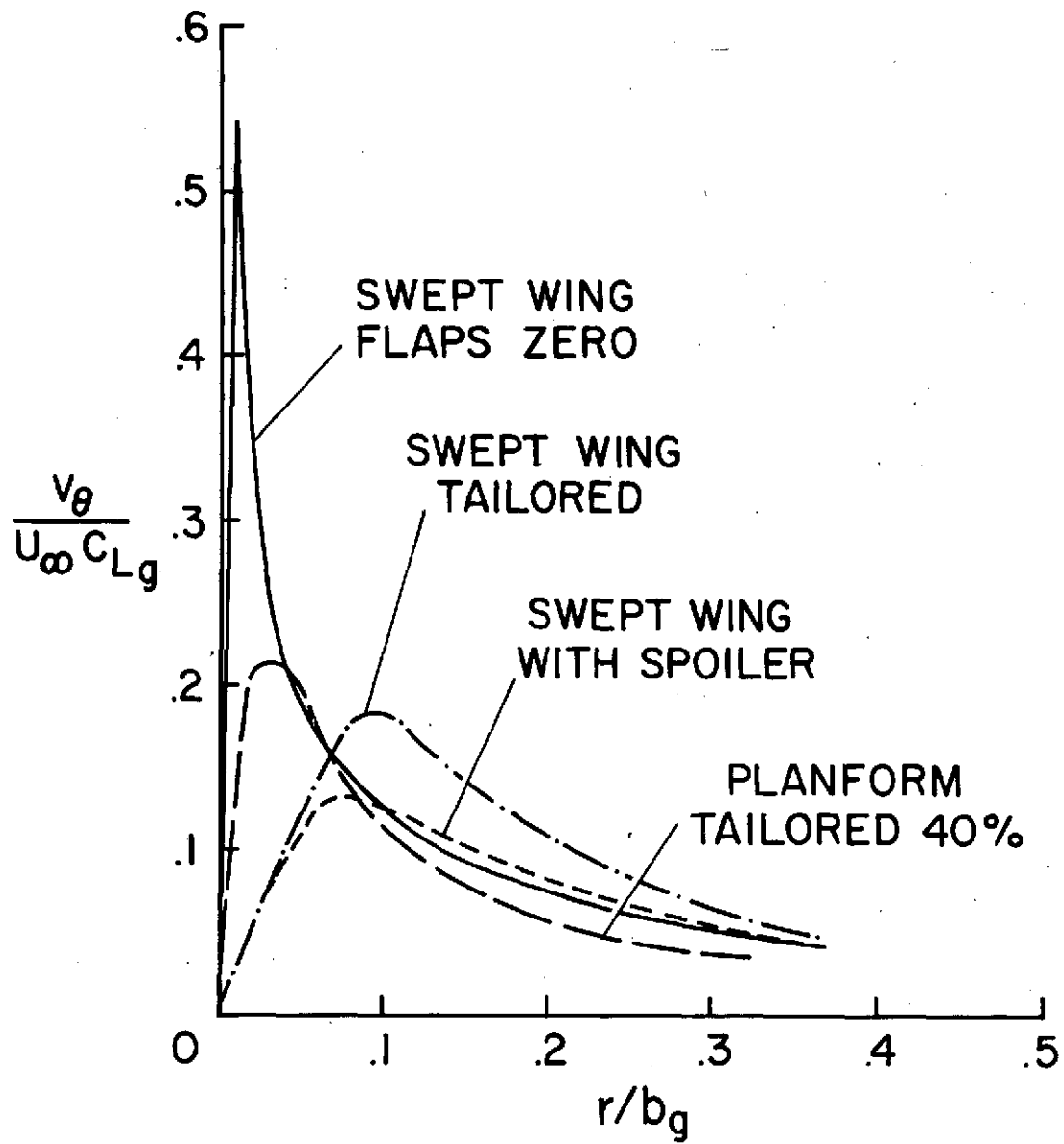
Figure 9.— Circumferential velocity profiles measured in wake vortices.

$$y_l = r_l + \int_0^{r_l} \frac{d(rv_\theta)}{v_\theta}$$

$$r_l = -\frac{1}{\Gamma_w(y_l)} \int_{b/2}^{y_l} \Gamma_w(y)\,dy$$
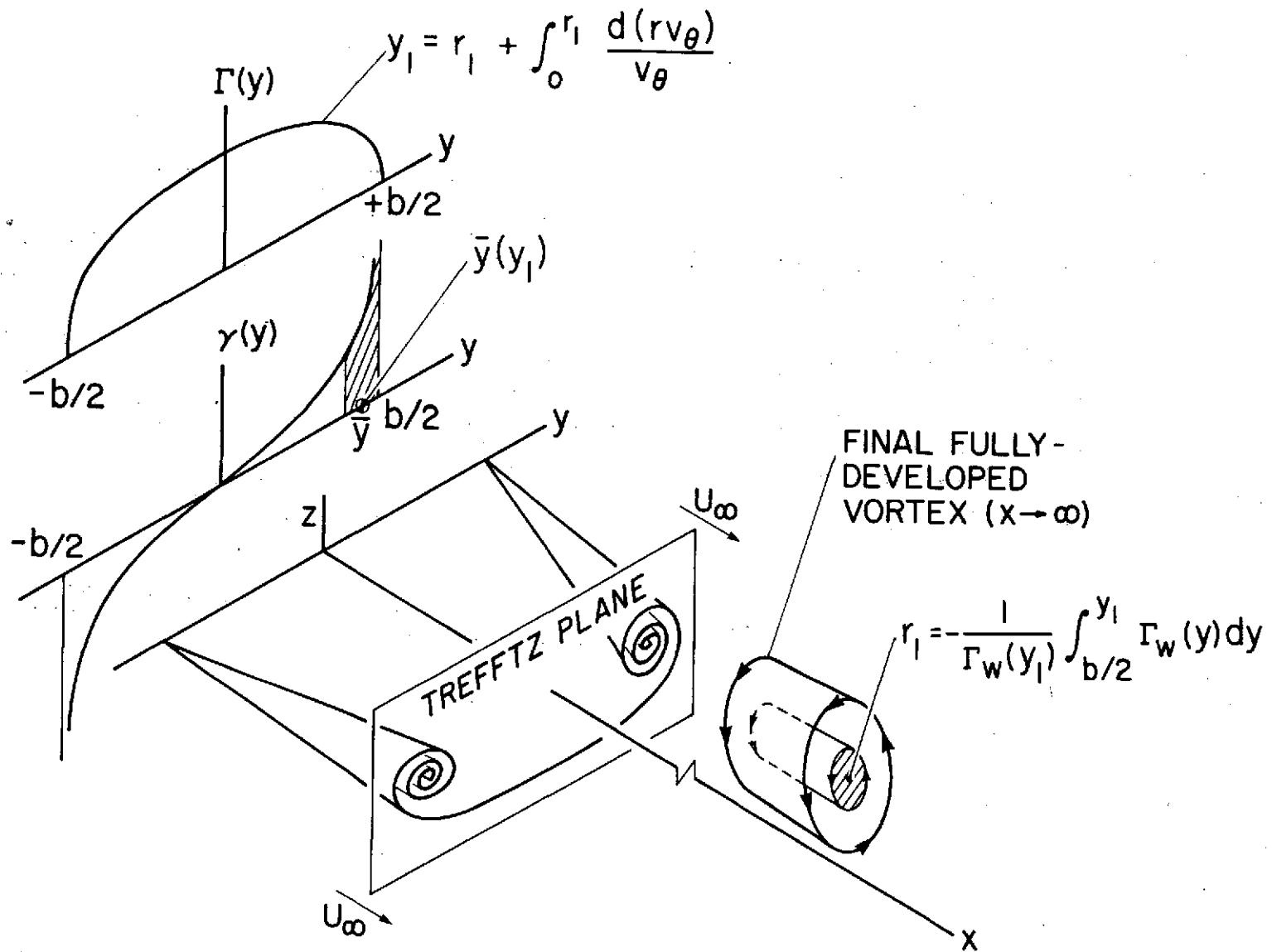
Figure 10.— Schematic diagram of wake rollup with relationships between span loading and vortex structure given for both direct- and inverse-rollup theories.
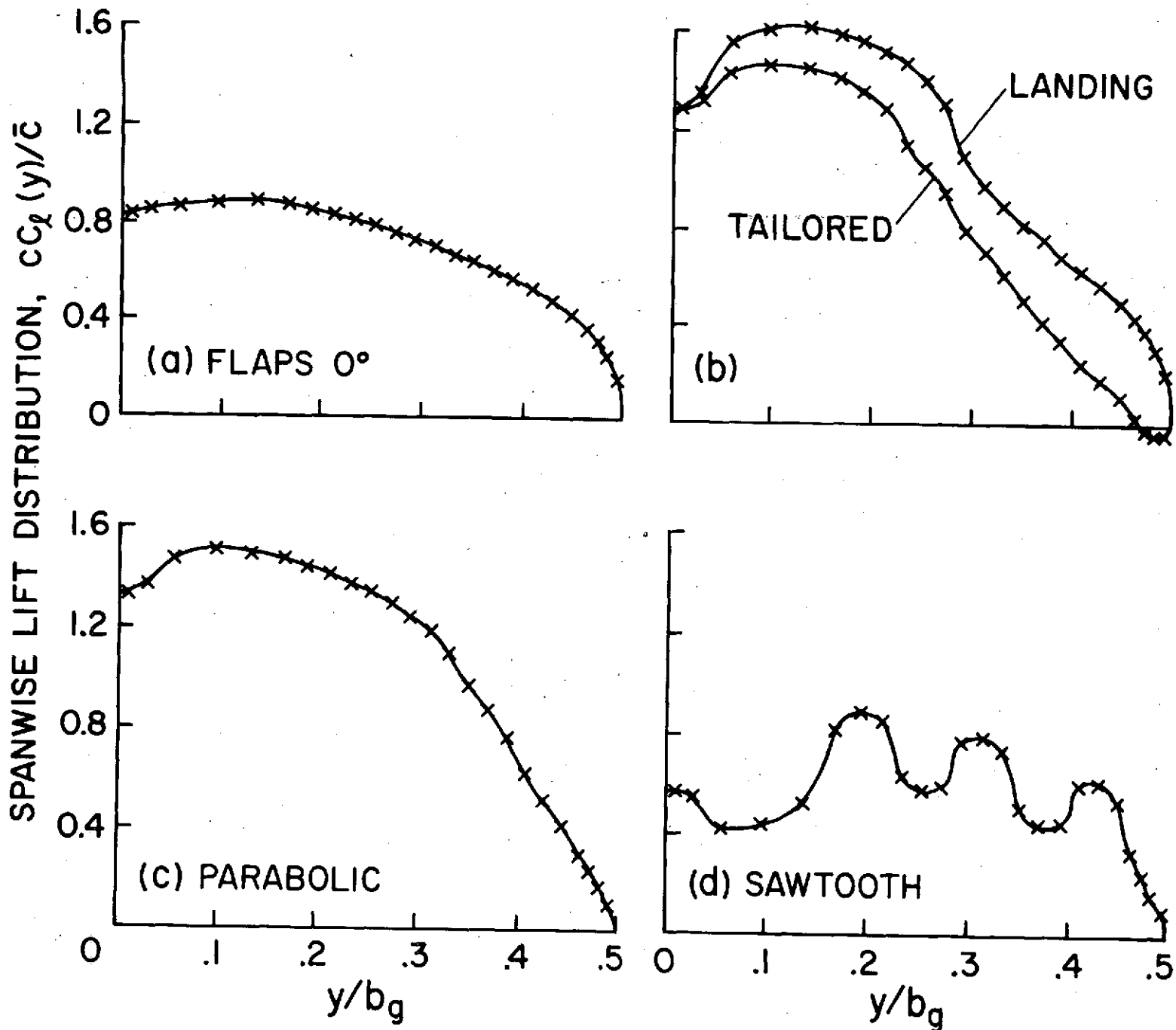
Figure 11.— Span loading on a swept wing as predicted by vortex-lattice theory.
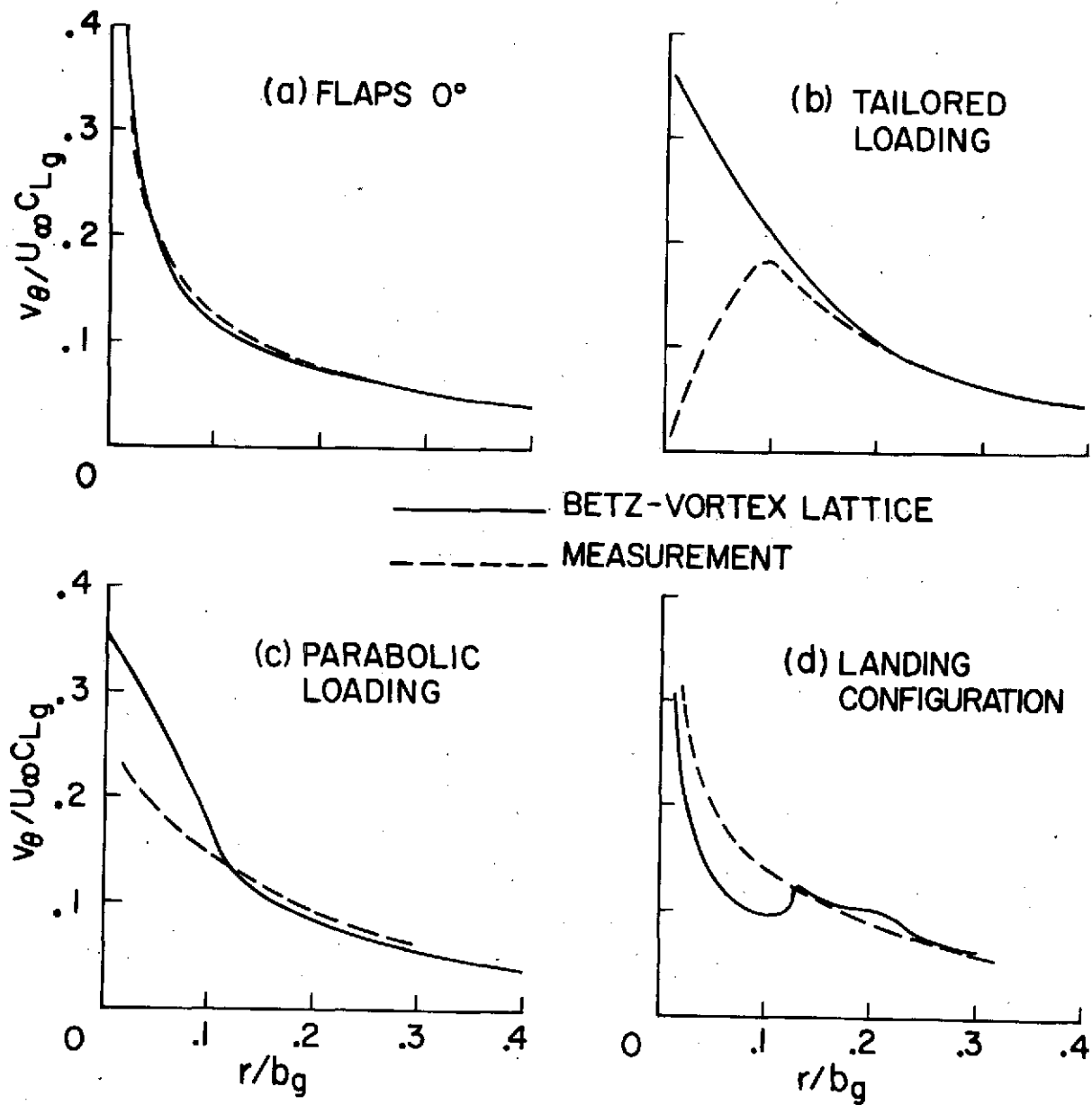
Figure 12.— Comparison of the measured circumferential velocity in the vortex with that predicted by the direct Betz rollup method using theoretical span-loading data given in figure 11.
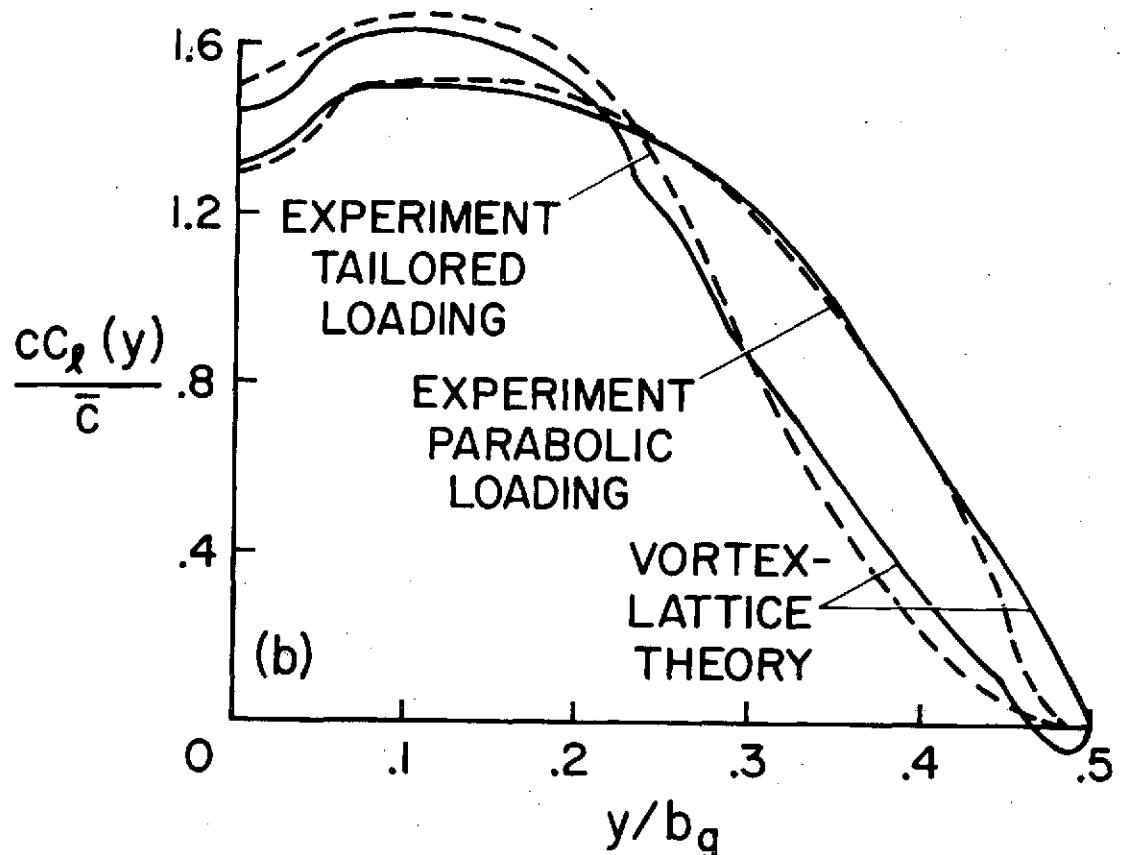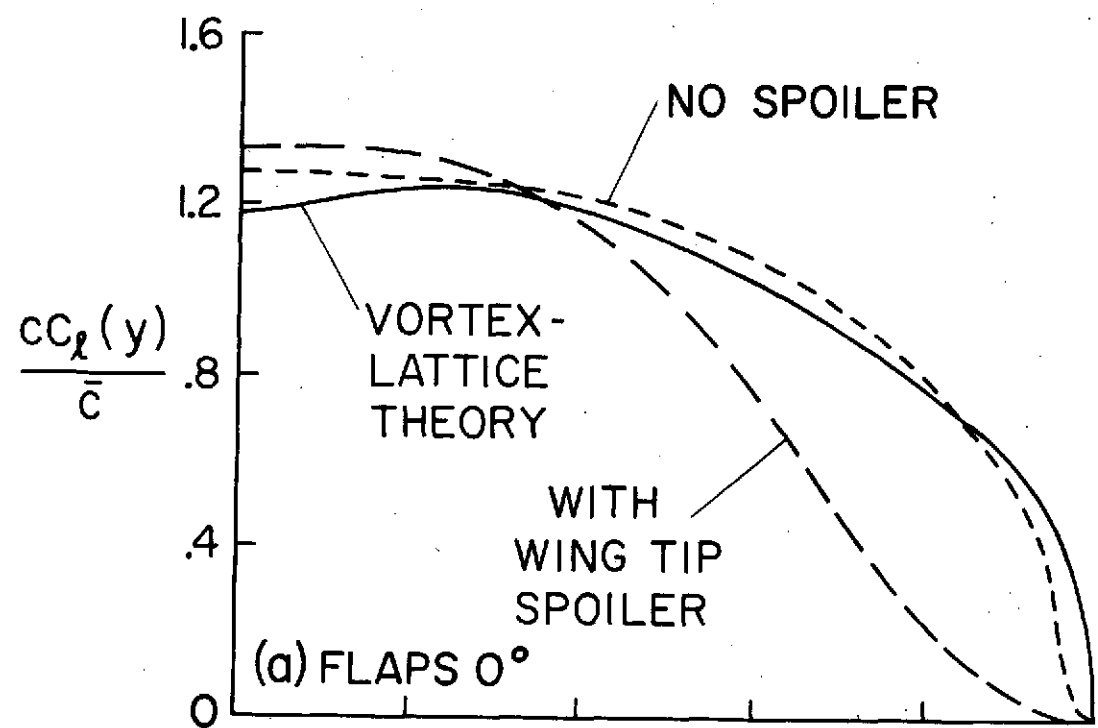
Figure 13.— Comparison of span loading predicted by vortex-lattice theory with that predicted by the inverse-rollup theory, which used measured vortex structure.
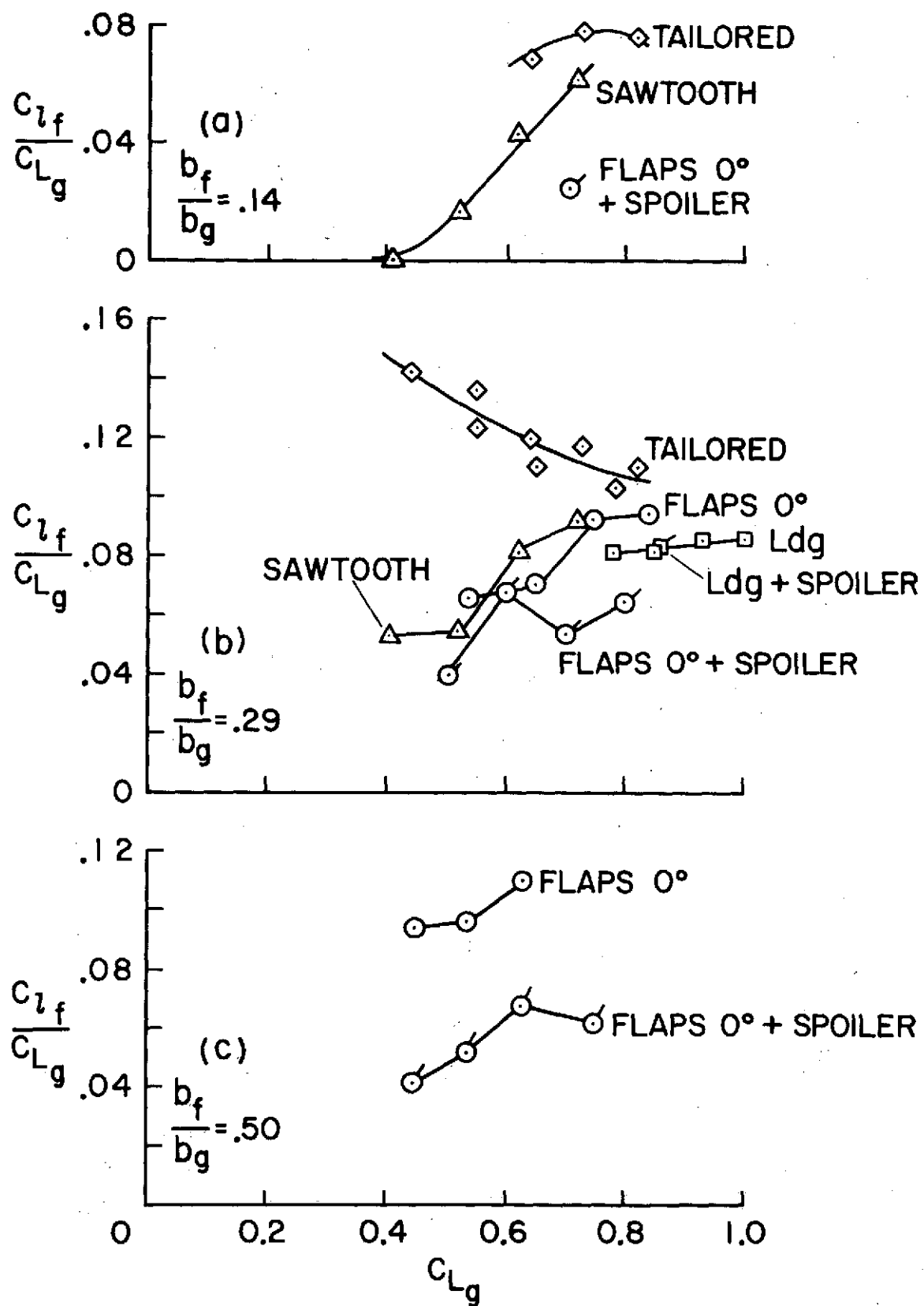
Figure 14.— Rolling-moment parameter as a function of lift on a swept-wing generator for various configurations tested.
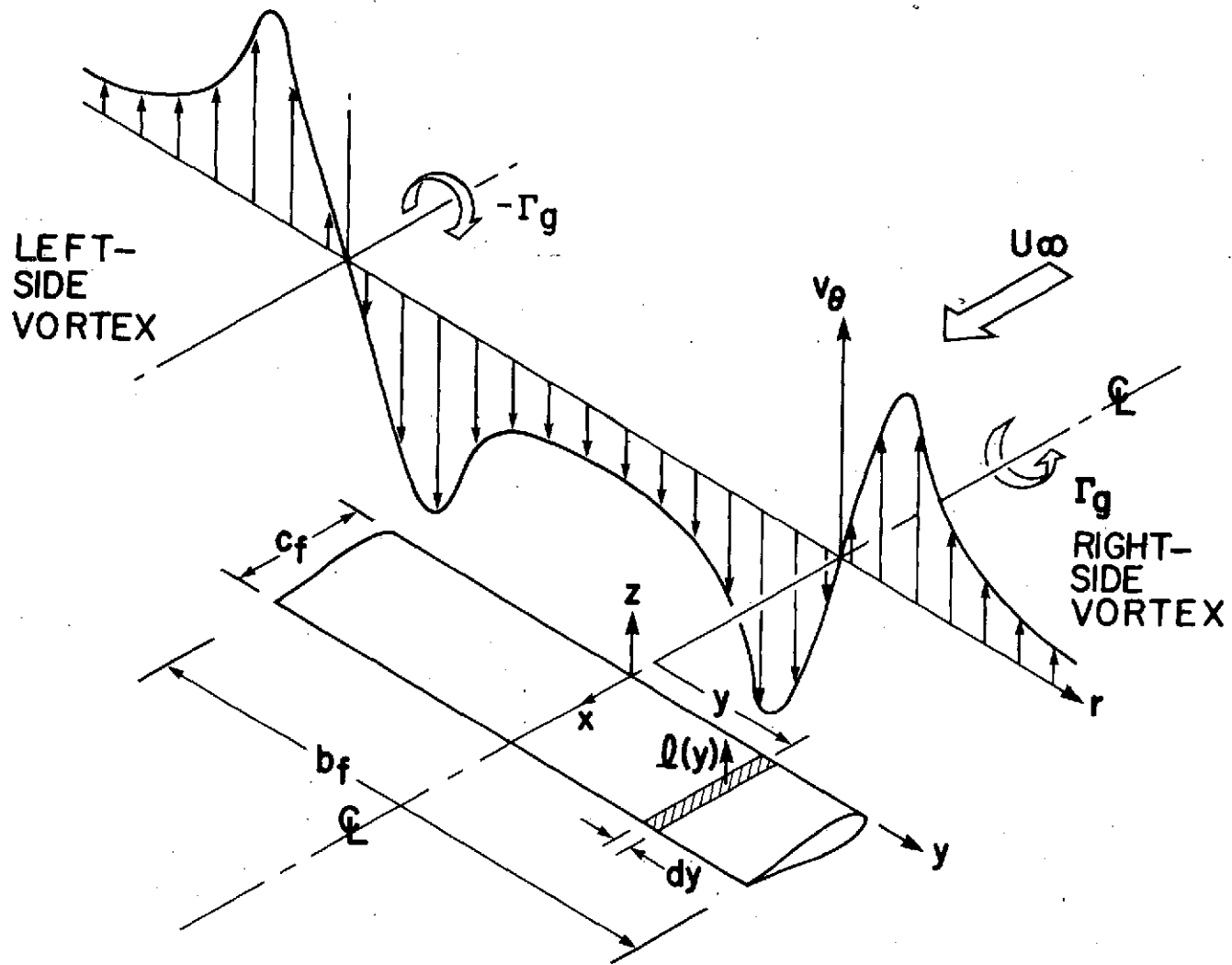
Figure 15.— Wake vortex impinging on a follower wing.
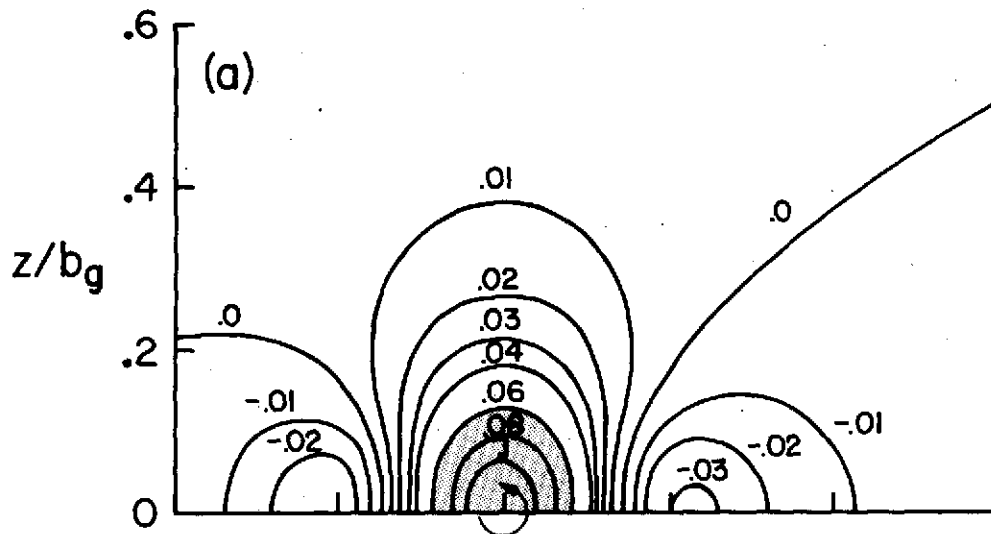
(a) Contours of equal rolling-moment parameter, C_{l_f}/C_{L_g}; $C_{l_f})_{max}/C_{L_g} = 0.122$.
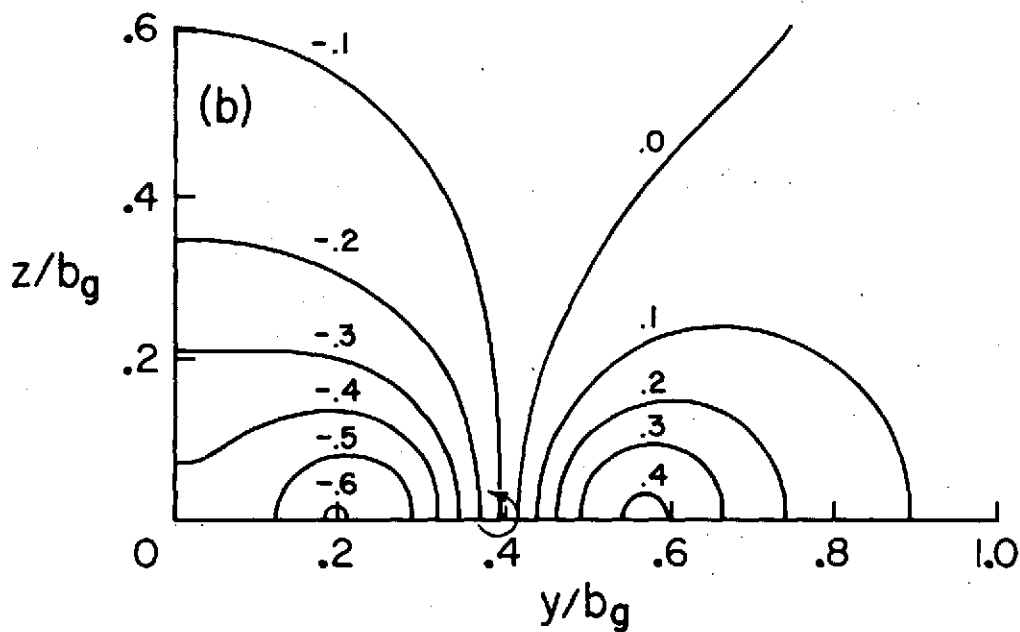
(b) Contours of equal lift parameter, C_{L_f}/C_{L_g}; $C_{L_f})_{max}/C_{L_g} = -0.88$.

Figure 16.— Rolling moment and lift induced on the follower wing by the wake of a swept wing; tailored loading, $b_f/b_g = 0.29$.